

Electroproduction of single pions at low ϵ and a measurement of the pion form factor up to $Q^2 = 10 \text{ GeV}^2$

C. J. Bebek, C. N. Brown,* S. D. Holmes,[†] R. V. Kline, F. M. Pipkin, S. Raither, and L. K. Sisterson[†]
High Energy Physics Laboratory, Harvard University, Cambridge, Massachusetts 02138

A. Browman,[§] K. M. Hanson,[§] D. Larson, and A. Silverman
Laboratory of Nuclear Studies, Cornell University, Ithaca, New York 14850
 (Received 13 June 1977; revised manuscript received 14 December 1977)

We report measurements of the electroproduction of single charged pions from hydrogen and deuterium targets for values of ϵ in the range $0.35 < \epsilon < 0.45$. Data were taken with a hydrogen target at the (W, Q^2) points (2.15 GeV, 1.2 GeV²), (2.65, 2.0), (2.65, 3.4), (2.65, 6.0), and (2.65, 10.0). Data were taken with a deuterium target at the (W, Q^2) points (2.15, 1.2) and (2.65, 2.0). The transverse cross section obtained by using these data in conjunction with earlier data at high ϵ to separate the longitudinal and transverse components is used in conjunction with the new data and the t -channel Born term to determine the pion form factor and to re-evaluate previously reported measurements. In the range $0.15 \text{ GeV}^2 < Q^2 < 10.0 \text{ GeV}^2$ the pion form factor can be described by the simple pole form $[1 + Q^2/(0.462 \pm 0.024)]^{-1}$.

I. INTRODUCTION

The electromagnetic structure of the pion has been the subject of numerous experimental and theoretical investigations.¹ It is described in terms of a single structure function or form factor which depends only on the square of the four-momentum transfer to the pion, Q^2 . Colliding-beam experiments measure the form factor in the time-like region $Q^2 < 0$ via the reaction

$$e^+e^- \rightarrow \pi^+\pi^-.$$

Pion scattering from atomic electrons

$$\pi e^- \rightarrow \pi e^-$$

gives a measurement of the pion form factor for small spacelike momentum transfers, $Q^2 > 0$. In both cases, the cross sections are directly proportional to the absolute square of the pion form factor and the extraction of $F_\pi(Q^2)$ is straightforward. The electroproduction of pions from nucleons

$$ep \rightarrow e\pi^+n, \quad (1a)$$

$$en \rightarrow e\pi^-p \quad (1b)$$

are the only available reactions that give information on the pion structure at large spacelike momentum transfers. The presence of the nucleons and their structure complicates theoretical models used to extract $F_\pi(Q^2)$ from the measurements and thus the determination of the pion form factor becomes model dependent.

In this paper, we report measurements of reactions (1) for small values of the virtual-photon polarization parameter ϵ ($0.30 < \epsilon < 0.45$) with values of the virtual-photon mass squared, $-Q^2$, extending up to 10 GeV^2 . These measurements were

carried out at the Wilson Synchrotron Laboratory at Cornell University. Cross sections and angular distributions for some of the data ($Q^2 \leq 3.3 \text{ GeV}^2$) have already been presented in an earlier paper.² In this paper, we give a complete report on the results of the experiment and report an analysis which gives a determination of the pion form factor over the full range of spacelike Q^2 up to 10 GeV^2 . These measurements represent a continuation of similar measurements at lower Q^2 by some members of the group. Hence we will rely on previous³⁻⁵ reports to supply background material for the kinematics, experimental techniques, and analysis procedures.

II. EXPERIMENT

Figure 1 is a schematic drawing of the spectrometer system used in this experiment. Two large-aperture (8-msr hadron arm and 40-msr electron arm) magnetic spectrometers were used to detect the scattered electron in coincidence with a charged hadron. The hadron-arm components included a large bending magnet, a multiwire-proportional-chamber system consisting of four x and four y planes of wires, four planes of plastic scintillator, a four-foot-diameter Freon-12 Čerenkov counter, and a 12-radiation-length lead-Lucite shower counter. In addition to a bending magnet the electron arm included six wire spark chambers equipped with magnetrostrictive readout, three planes of scintillation counters, a five-foot-diameter Freon-12 Čerenkov counter, and a 12-radiation-length lead-Lucite shower counter.

Table I summarizes the points at which data were taken and gives the nominal W (total center-of-mass energy), Q^2 , and ϵ (photon polarization

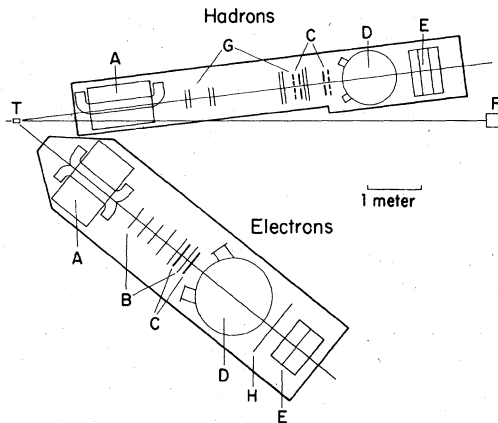


FIG. 1. Plan view of the apparatus consisting of (A) bending magnets, (B) spark chambers, (C) scintillation counters, (D) Freon gas Čerenkov counters, (E) lead-Lucite shower counters, (F) Faraday cup, (G) multi-wire proportional chambers, (H) scintillation counter hodoscope, (T) production target.

parameter) for each of the data points. The two spectrometer arms were arranged so that the hadron arm was centered along the direction of the virtual photon. Thus the acceptance was peaked at $\theta = 0^\circ$ in the virtual-photon-nucleon center-of-mass system.

The trigger required counts in three of the four planes of scintillator on the hadron arm and counts in the first two planes of scintillator, the Čerenkov counter, and the shower counter on the electron arm. The hadron-arm shower counter was used off-line to reject electrons counting in the hadron arm when detecting negatively charged particles. The hadron arm Čerenkov counter served to separate pions from protons and kaons at momenta greater than $1.8 \text{ GeV}/c$. At lower momenta, particle identification was made using time of flight.

For a typical data point, the data were corrected for counter dead times $[(5 \pm 2)\%]$, wire-chamber inefficiencies $[(1.5 \pm 0.5)\%]$, electron-shower-counter inefficiency $[(1 \pm 1)\%]$, pion absorption $[(5 \pm 1)\%]$, hadron-arm Čerenkov-counter inefficiency and absorption of pions above threshold $[(10 \pm 2)\%]$, pion

TABLE I. The nominal kinematic points at which data were taken.

Data point	Targets	W (GeV)	Q^2 (GeV ²)	ϵ
1	H ₂ , D ₂	2.15	1.2	0.45
2	H ₂ , D ₂	2.65	2.0	0.35
3	H ₂	2.65	3.3	0.40
4	H ₂	2.65	6.2	0.40
5	H ₂	2.65	10.0	0.40

decay $[(3 \pm 1)\%]$, and proton contamination due to knock-on events which fired the Čerenkov counter $[(5 \pm 1)\%]$. Target-wall events were subtracted using data taken with an empty target. The correction for target-wall events was typically $(2 \pm 1)\%$. In each case the first number represents the typical correction and the second number represents the uncertainty in the correction.

An arm-to-arm time-of-flight system with a Gaussian σ of 0.4 nsec for pions was used to select in-time events and reject random events. Events within ± 1.5 nsec of the expected time of flight were taken as in-time events and an out-of-time interval with a width of 3 nsec was used to correct for random coincidences. Randoms were typically $(2 \pm 1)\%$; in-time pion losses due to the timing cuts were typically $(1 \pm 1)\%$.

The measured cross sections were also corrected for losses due to the radiation of photons. The prescription for the radiative correction was taken from the work of Bartl and Urban.⁶ The full radiative correction varied from 28 to 51% over the range of the data points reported here. The explicit radiative correction has been listed for each bin in the tables. It is estimated that the uncertainty in the radiative correction results in an uncertainty of $\pm 2\%$ in the final corrected cross sections.

The acceptance was determined by a Monte Carlo calculation assuming a unit cross section and incorporating multiple scattering, detector resolution, and geometrical effects. The overall normalization of the experiment was checked by observing elastic electron scattering independently with each of the arms. The mean ratios of the measured elastic scattering cross sections to the average of the world data for the electron and the hadron arms were 0.972 ± 0.010 and 0.993 ± 0.040 ,

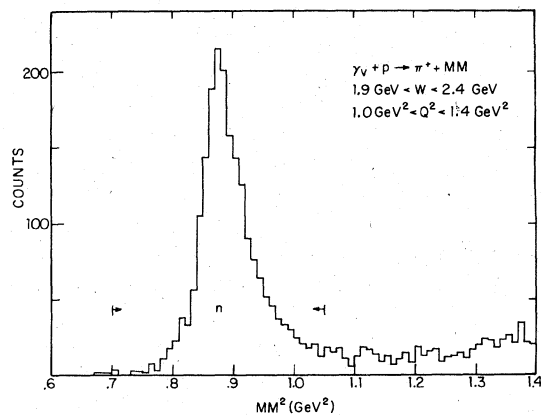


FIG. 2. Missing-mass-squared distribution for the reaction $\gamma_\nu + p \rightarrow \pi^+ + \text{MM}$ for $1.9 \text{ GeV} < W < 2.4 \text{ GeV}$ and $1.0 \text{ GeV}^2 < Q^2 < 1.4 \text{ GeV}^2$.

TABLE II. A summary of the corrections to a typical data point and the contributions to the overall systematic uncertainty in the normalization.

Correction	Magnitude (%)	Uncertainty (%)
Counter deadtime	5	± 2
Wire-chamber inefficiencies	1.5	± 0.5
Electron-shower-counter inefficiency	1	± 1
Pion absorption	5	± 1
Hadron-Cerenkov-counter inefficiency	10	± 2
Pion decay	3	± 1
Proton contamination	5	± 1
Target out	2	± 1
Random events	2	± 1
Pion loss due to timing cuts	1	± 1
Radiative correction	40	± 2
Quadratic sum of uncertainties		± 4.4
Uncertainty suggested by electron scattering calibration		-3
Quadratic sum		± 5.3

respectively.

The invariant undetected mass squared was calculated from measurements of the incident and scattered electron momenta and the momentum of the electroproduced hadron. Figure 2 shows the missing-mass-squared distribution for pion events taken from the lowest- Q^2 point. A clear peak is seen at the missing mass squared corresponding to an undetected neutron. A cut at $0.7 < MM^2 < 1.05$ GeV² was used to separate out events corresponding to reaction (1a).

The uncertainties quoted in the data are statistical only and do not include a possible overall systematic uncertainty. It is estimated that the overall systematic uncertainty is less than 6%. This estimate is based on the errors in the corrections to the data, the uncertainty in the radiative correction, and the discrepancy in the electron scattering normalization measurements. Table II summarizes the various contributions to the overall systematic uncertainty. For a more complete discussion of the various contributions the reader should consult Refs. 4 and 5 and especially Ref. 3. The apparatus itself and the peculiarities of this particular configuration are treated more completely in the paper reporting measurements of the inclusive pion cross section.⁷

III. RESULTS

Reactions (1) are analyzed in terms of the virtual-photon production reactions⁸

$$\begin{aligned} \gamma_\nu p &\rightarrow \pi^+ n, \\ \gamma_\nu p &\rightarrow \pi^- p. \end{aligned} \quad (2)$$

The most general form of the cross section for reactions (2) is written

$$\frac{d\sigma}{d\Omega} = A + \epsilon C + \epsilon \cos 2\phi B + \left[\frac{\epsilon(\epsilon+1)}{2} \right]^{1/2} (\cos\phi) D, \quad (3)$$

where A , B , C , and D are functions of the center-of-mass variables W , θ (angle between photon and pion), and Q^2 . The dependence on the azimuth ϕ is displayed explicitly by Eq. (3). A represents the cross section for transverse photons, C the cross section for longitudinal photons, B the interference between the transverse amplitudes, and D the interference between the transverse and longitudinal amplitudes. The terms B and D approach zero as $\theta \rightarrow 0$ and the terms C and D vanish as $Q^2 \rightarrow 0$.

Tables III(a) through III(e) list the π^*n cross sections for a hydrogen target determined in this experiment. For the deuterium target, the π^*n cross sections are listed in Tables IV(a) and IV(b), while the π^*p cross sections appear in Tables V(a) and V(b). The deuterium data have not been corrected for events which are not identified with reactions (2) due to the Fermi motion of the nucleons. A calculation based on the Hulthén⁹ wave function indicates that this effect is less than 0.5%. Since there is a high correlation of the average virtual-photon and pion directions, the average values of the virtual-photon parameters over the events in the bin are also included for each bin.

A number of theories¹⁰⁻¹⁵ have been advanced to describe the electroproduction of π^*n for pions emitted along the virtual-photon direction and to predict the terms A , B , C , and D in Eq. (3). Most of them succeed in describing the general features of the cross section, but none of them is sufficiently refined to give total confidence in the determination of the pion form factor which enters in the models as a free parameter. The common ingredient in all the theoretical models is the t -channel pion-exchange graph which is the main contributor to the amplitude due to longitudinally polarized photons. This amplitude is directly proportional to the pion form factor and is easily evaluated in the Born approximation. The portion of the amplitude due to transversely polarized photons is subject to large theoretical uncertainties. In dispersion-theory models,¹⁰⁻¹² it is given by the s - and u -channel Born terms, dispersion-integral corrections, and, for $\theta > 0^\circ$, the t -channel Born term.

In an earlier paper,² we presented the first measurements of the separated transverse and longitudinal cross sections, terms A and C in Eq. (3).

TABLE III. The bins and the center-of-mass virtual-photoproduction cross sections for the reaction $\gamma_p + p \rightarrow \pi^+ + n$ off a hydrogen target. The uncertainties are statistical only. N is the number of events in the bin. The cross sections shown have been radiatively corrected by multiplying the measured cross sections with the factor RAD.

ϕ (deg)	θ (deg)	$\frac{d\sigma}{d\Omega_r}$ ($\frac{\mu\text{b}}{\text{sr}}$)	θ (deg)	W (GeV)	Q^2 (GeV ²)	ϵ	$\epsilon \cos 2\phi$	$\left[\frac{\epsilon(\epsilon+1)}{2}\right]^{1/2}$	$\cos \phi$	t (GeV ²)	RAD	N
(a) Data point 1 (H ₂)												
All	0-3	2.97 ± 0.27	1.97	2.111	1.179	0.466	-0.008	0.022	-0.07	1.325	154	
(-135)-(-45)	0-3	3.56 ± 0.61	2.08	2.112	1.160	0.470	-0.305	0.037	-0.08	1.322	46	
	3-6	2.55 ± 0.30	4.49	2.116	1.200	0.457	-0.336	-0.014	-0.08	1.321	92	
	6-9	2.97 ± 0.30	7.50	2.125	1.184	0.449	-0.300	-0.010	-0.09	1.319	128	
	9-12	2.47 ± 0.27	10.39	2.119	1.194	0.451	-0.309	-0.006	-0.11	1.318	108	
	12-15	2.31 ± 0.29	13.50	2.127	1.175	0.451	-0.286	0.007	-0.13	1.318	80	
	15-18	2.40 ± 0.36	16.34	2.084	1.233	0.473	-0.324	0.077	-0.17	1.319	52	
	18-21	2.10 ± 0.51	18.88	2.074	1.234	0.484	-0.306	0.147	-0.19	1.323	19	
	21-24	2.22 ± 1.19	21.60	2.078	1.238	0.479	-0.148	0.206	-0.24	1.325	4	
(-45)-(45)	0-3	3.13 ± 0.56	1.90	2.092	1.205	0.475	0.312	0.537	-0.08	1.324	40	
	3-6	3.21 ± 0.36	4.47	2.071	1.226	0.490	0.306	0.542	-0.09	1.329	96	
	6-9	2.97 ± 0.33	7.39	2.025	1.273	0.518	0.330	0.564	-0.11	1.333	105	
	9-12	2.71 ± 0.32	10.53	1.995	1.299	0.535	0.346	0.578	-0.13	1.338	86	
	12-15	2.05 ± 0.34	13.40	1.971	1.329	0.547	0.264	0.557	-0.16	1.342	46	
	15-18	1.25 ± 0.34	16.09	1.956	1.348	0.557	0.276	0.566	-0.19	1.347	15	
	18-21	0.70 ± 0.42	19.06	1.953	1.301	0.562	0.331	0.590	-0.21	1.351	3	
	21-24	3.23 ± 1.77	22.34	1.957	1.350	0.558	0.077	0.497	-0.25	1.355	4	
(45)-(135)	0-3	2.25 ± 0.47	2.05	2.124	1.161	0.458	-0.307	-0.028	-0.07	1.321	31	
	3-6	3.21 ± 0.33	4.62	2.106	1.183	0.467	-0.291	0.029	-0.08	1.321	115	
	6-9	2.78 ± 0.28	7.56	2.103	1.195	0.467	-0.303	0.023	-0.09	1.320	143	
	9-12	2.48 ± 0.25	10.40	2.104	1.204	0.464	-0.311	0.044	-0.11	1.320	112	
	12-15	2.08 ± 0.27	13.19	2.117	1.209	0.452	-0.326	-0.003	-0.13	1.318	67	
	15-18	2.71 ± 0.45	16.47	2.106	1.171	0.471	-0.329	0.052	-0.15	1.319	46	
	18-21	1.89 ± 0.66	19.11	2.107	1.195	0.458	-0.289	0.074	-0.18	1.318	9	
(135)-(225)	0-3	2.93 ± 0.52	1.94	2.118	1.189	0.458	0.265	-0.510	-0.07	1.318	37	
	3-6	2.63 ± 0.30	4.54	2.167	1.126	0.426	0.268	-0.494	-0.07	1.313	95	
	6-9	2.43 ± 0.26	7.51	2.173	1.120	0.421	0.232	-0.479	-0.08	1.306	97	
	9-12	2.06 ± 0.27	10.41	2.200	1.100	0.400	0.226	-0.465	-0.10	1.300	80	
	12-15	1.86 ± 0.33	13.16	2.227	1.068	0.379	0.225	-0.454	-0.11	1.294	34	
	15-18	0.43 ± 0.26	16.51	2.248	1.067	0.360	0.084	-0.387	-0.13	1.286	3	
	18-21	1.05 ± 1.07	18.85	2.316	1.002	0.309	0.280	-0.439	-0.17	1.280	1	
(b) Data point 2 (H ₂)												
All	0-3	1.26 ± 0.15	2.00	2.667	1.942	0.334	-0.021	0.043	-0.07	1.405	87	
(-135)-(-45)	0-3	1.27 ± 0.29	2.13	2.696	1.894	0.322	-0.222	0.071	-0.06	1.403	21	
	3-6	0.96 ± 0.16	4.58	2.656	1.987	0.334	-0.189	0.048	-0.08	1.400	46	
	6-9	0.88 ± 0.13	7.53	2.660	1.960	0.337	-0.208	0.064	-0.10	1.401	49	
	9-12	0.96 ± 0.15	10.54	2.663	1.954	0.335	-0.203	0.043	-0.13	1.399	46	
	12-15	0.61 ± 0.15	13.56	2.632	2.044	0.338	-0.201	0.112	-0.18	1.401	18	
	15-18	0.43 ± 0.23	16.04	2.503	2.282	0.408	-0.251	0.223	-0.25	1.407	6	
	18-21	0.94 ± 0.97	18.36	2.609	2.019	0.387	-0.152	0.286	-0.31	1.422	1	
(-45)-(45)	0-3	1.19 ± 0.28	2.07	2.641	1.980	0.349	0.242	0.444	-0.07	1.406	20	
	3-6	1.13 ± 0.19	4.45	2.594	2.091	0.371	0.214	0.445	-0.10	1.411	55	
	6-9	1.01 ± 0.16	7.50	2.564	2.145	0.384	0.242	0.463	-0.12	1.419	55	
	9-12	0.91 ± 0.15	10.34	2.525	2.218	0.407	0.265	0.483	-0.16	1.426	42	
	12-15	0.53 ± 0.17	13.12	2.490	2.242	0.423	0.232	0.481	-0.20	1.430	16	
	15-18	0.57 ± 0.22	16.26	2.470	2.284	0.426	0.211	0.475	-0.23	1.436	7	
	18-21	1.15 ± 0.60	19.40	2.466	2.289	0.441	0.169	0.465	-0.29	1.447	4	

TABLE III. (Continued)

ϕ (deg)	θ (deg)	$\frac{d\sigma}{d\Omega_\pi} \left(\frac{\mu\text{b}}{\text{sr}} \right)$	θ (deg)	W (GeV)	Q^2 (GeV ²)	ϵ	$\epsilon \cos 2\phi$	$\left[\frac{\epsilon(\epsilon+1)}{2} \right]^{1/2} \cos \phi$	t (GeV ²)	RAD	N
(b) Data point 2 (H ₂)											
(45)-(135)	0-3	1.57 ± 0.33	1.89	2.624	2.053	0.352	-0.252	0.067	-0.08	1.400	26
	3-6	1.31 ± 0.18	4.57	2.643	1.982	0.351	-0.205	0.026	-0.09	1.401	56
	6-9	0.69 ± 0.12	7.53	2.654	1.946	0.344	-0.246	0.022	-0.11	1.400	44
	9-12	0.99 ± 0.15	10.22	2.639	1.988	0.353	-0.211	0.124	-0.14	1.405	53
	12-15	0.61 ± 0.14	13.63	2.623	2.037	0.357	-0.208	0.147	-0.19	1.406	21
	15-18	0.54 ± 0.22	16.11	2.623	2.081	0.347	-0.177	0.117	-0.24	1.403	6
18-21	1.05 ± 0.77	18.34	2.525	2.279	0.383	-0.159	0.278	-0.32	1.414	2	
(135)-(225)	0-3	0.99 ± 0.32	1.92	2.718	1.812	0.309	0.229	-0.417	-0.05	1.396	20
	3-6	1.28 ± 0.21	4.20	2.697	1.904	0.314	0.197	-0.407	-0.08	1.388	43
	6-9	0.51 ± 0.13	7.56	2.713	1.857	0.311	0.153	-0.388	-0.10	1.380	24
	9-12	0.76 ± 0.18	10.27	2.757	1.741	0.287	0.184	-0.388	-0.11	1.371	20
	12-15	0.26 ± 0.15	13.62	2.803	1.627	0.270	0.159	-0.368	-0.13	1.365	3
(c) Data point 3 (H ₂)											
All	0-3	0.52 ± 0.10	1.92	2.625	3.330	0.395	-0.000	0.102	-0.17	1.430	35
(-135)-(-45)	0-3	0.41 ± 0.17	1.44	2.722	3.037	0.383	-0.238	0.166	-0.13	1.434	7
	3-6	0.59 ± 0.12	4.83	2.678	3.235	0.378	-0.248	-0.065	-0.17	1.427	32
	6-9	0.57 ± 0.09	7.53	2.621	3.355	0.398	-0.264	0.023	-0.21	1.426	45
	9-12	0.46 ± 0.07	10.73	2.641	3.358	0.384	-0.263	-0.084	-0.24	1.420	43
	12-15	0.43 ± 0.07	13.62	2.636	3.352	0.384	-0.255	0.014	-0.28	1.424	43
	15-18	0.35 ± 0.08	16.46	2.643	3.334	0.386	-0.287	0.041	-0.34	1.427	31
	18-21	0.31 ± 0.08	19.41	2.626	3.354	0.390	-0.266	0.008	-0.41	1.421	18
	21-24	0.29 ± 0.12	22.28	2.606	3.484	0.385	-0.297	0.041	-0.51	1.422	14
24-27	0.20 ± 0.13	25.54	2.624	3.598	0.367	-0.253	0.024	-0.62	1.420	3	
(-45)-(45)	0-3	0.75 ± 0.23	1.89	2.608	3.377	0.395	0.224	0.463	-0.17	1.429	12
	3-6	0.53 ± 0.12	4.42	2.573	3.396	0.420	0.234	0.479	-0.20	1.436	28
	6-9	0.62 ± 0.11	7.30	2.541	3.533	0.428	0.255	0.491	-0.24	1.443	38
	9-12	0.48 ± 0.10	10.62	2.501	3.652	0.438	0.281	0.505	-0.29	1.450	27
	12-15	0.32 ± 0.09	13.33	2.482	3.696	0.438	0.242	0.491	-0.33	1.455	17
	15-18	0.49 ± 0.14	16.21	2.458	3.781	0.453	0.274	0.511	-0.41	1.463	14
	18-21	0.20 ± 0.12	19.90	2.457	3.716	0.453	0.222	0.494	-0.51	1.463	3
	21-24	0.44 ± 0.32	22.01	2.439	3.813	0.455	0.111	0.453	-0.55	1.477	2
(45)-(135)	0-3	0.46 ± 0.15	2.00	2.599	3.407	0.398	-0.197	-0.051	-0.18	1.423	10
	3-6	0.48 ± 0.10	4.52	2.661	3.305	0.378	-0.236	-0.031	-0.18	1.426	27
	6-9	0.62 ± 0.10	7.53	2.627	3.385	0.391	-0.266	0.004	-0.22	1.425	55
	9-12	0.64 ± 0.09	10.46	2.647	3.346	0.383	-0.268	-0.012	-0.25	1.425	61
	12-15	0.53 ± 0.08	13.56	2.646	3.323	0.387	-0.315	0.020	-0.29	1.426	49
	15-18	0.36 ± 0.07	16.24	2.666	3.224	0.385	-0.248	-0.010	-0.33	1.423	29
	18-21	0.31 ± 0.08	19.35	2.581	3.567	0.396	-0.219	0.142	-0.45	1.433	16
	21-24	0.39 ± 0.13	22.38	2.624	3.482	0.386	-0.243	0.131	-0.52	1.435	10
24-27	0.17 ± 0.19	24.13	2.599	3.628	0.385	-0.309	0.162	-0.59	1.438	1	
(135)-(225)	0-3	0.47 ± 0.27	2.39	2.589	3.451	0.402	0.159	-0.440	-0.20	1.418	6
	3-6	0.61 ± 0.16	4.70	2.714	3.184	0.354	0.222	-0.439	-0.16	1.416	19
	6-9	0.55 ± 0.13	7.87	2.710	3.178	0.364	0.228	-0.447	-0.19	1.409	22
	9-12	0.65 ± 0.12	10.42	2.714	3.223	0.355	0.185	-0.426	-0.22	1.402	31
	12-15	0.14 ± 0.06	13.24	2.805	2.925	0.326	0.190	-0.412	-0.24	1.396	6
	15-18	0.41 ± 0.14	16.11	2.793	2.932	0.325	0.192	-0.411	-0.28	1.387	9
	18-21	0.12 ± 0.17	18.84	2.870	2.799	0.311	0.153	-0.388	-0.34	1.386	3
	21-24	0.77 ± 0.57	21.94	2.869	2.788	0.282	0.187	-0.387	-0.44	1.368	2

TABLE III. (Continued)

ϕ (deg)	θ (deg)	$\frac{d\sigma}{d\Omega_r} \left(\frac{\mu\text{b}}{\text{sr}} \right)$	θ (deg)	W (GeV)	Q^2 (GeV ²)	ϵ	$\epsilon \cos 2\phi$	$\left[\frac{\epsilon(\epsilon+1)}{2} \right]^{1/2} \cos \phi$	t (GeV ²)	RAD	N
(d) Data point 4 (H ₂)											
All	0-6	0.19 ± 0.05	4.16	2.660	6.297	0.400	-0.024	0.098	-0.43	1.476	25
(-135)-(-45)	0-6	0.08 ± 0.10	4.92	2.698	6.176	0.388	-0.316	-0.035	-0.43	1.465	5
	6-12	0.28 ± 0.06	8.79	2.646	6.240	0.412	-0.217	-0.023	-0.50	1.464	21
	12-18	0.27 ± 0.06	14.67	2.683	6.133	0.410	-0.258	-0.020	-0.58	1.465	20
	18-24	0.14 ± 0.07	19.95	2.631	6.513	0.397	-0.276	-0.137	-0.85	1.448	15
	24-30	0.09 ± 0.60	26.01	2.609	6.360	0.427	-0.391	0.112	-1.02	1.479	2
(-45)-(45)	0-6	0.23 ± 0.11	3.17	2.649	6.208	0.415	0.285	0.494	-0.42	1.475	8
	6-12	0.31 ± 0.09	8.50	2.533	6.604	0.430	0.285	0.502	-0.59	1.483	19
	12-18	0.10 ± 0.40	14.04	2.526	6.551	0.449	0.236	0.495	-0.65	1.500	4
	18-24	0.21 ± 0.12	19.68	2.502	6.513	0.458	0.260	0.510	-0.85	1.515	3
(45)-(135)	0-6	0.25 ± 0.09	4.30	2.609	6.432	0.415	-0.311	0.069	-0.47	1.465	8
	6-12	0.09 ± 0.70	8.86	2.701	6.343	0.378	-0.275	-0.069	-0.51	1.463	12
	12-18	0.17 ± 0.04	14.34	2.637	6.322	0.408	-0.263	-0.034	-0.65	1.460	20
	18-24	0.10 ± 0.03	20.91	2.642	6.384	0.396	-0.291	-0.088	-0.88	1.454	13
	24-30	0.12 ± 0.05	26.20	2.579	6.412	0.430	-0.302	0.139	-1.09	1.479	7
(135)-(225)	0-6	0.23 ± 0.12	4.92	2.736	6.355	0.358	0.300	-0.472	-0.38	1.453	4
	6-12	0.17 ± 0.07	8.43	2.724	6.175	0.383	0.243	-0.463	-0.50	1.445	9
	12-18	0.12 ± 0.05	14.64	2.761	5.830	0.390	0.175	-0.442	-0.56	1.432	6
	18-24	0.13 ± 0.08	19.27	2.806	6.074	0.341	0.214	-0.429	-0.71	1.414	3
(e) Data point 5 (H ₂)											
All	0-6	0.12 ± 0.03	4.14	2.635	9.770	0.400	0.089	0.119	-0.87	1.461	18
(-135)-(-45)	0-6	0.06 ± 0.10	5.18	2.508	10.096	0.433	-0.250	-0.068	-0.98	1.445	2
	6-12	0.06 ± 0.30	8.45	2.662	9.770	0.392	-0.331	-0.044	-0.98	1.451	7
	12-18	0.09 ± 0.30	14.81	2.662	9.743	0.383	-0.242	0.027	-1.06	1.456	13
	18-24	0.04 ± 0.80	20.17	2.565	9.998	0.413	-0.267	-0.035	-1.43	1.448	5
(-45)-(45)	0-6	0.25 ± 0.09	3.61	2.648	9.872	0.387	0.221	0.456	-0.87	1.463	9
	6-12	0.06 ± 0.40	9.13	2.632	9.692	0.405	0.240	0.475	-0.95	1.479	8
	12-18	0.07 ± 0.70	14.38	2.529	10.048	0.421	0.281	0.497	-1.15	1.490	8
	18-24	0.05 ± 0.80	19.78	2.600	9.353	0.438	0.242	0.488	-1.20	1.506	2
	24-30	0.08 ± 0.50	27.88	2.414	10.585	0.428	0.184	0.464	-1.96	1.511	2
(45)-(135)	0-6	0.08 ± 0.20	3.49	2.580	9.778	0.428	-0.212	-0.015	-0.87	1.450	3
	6-12	0.15 ± 0.04	9.64	2.718	9.509	0.387	-0.272	-0.127	-0.89	1.449	17
	12-18	0.04 ± 0.60	15.77	2.703	9.557	0.386	-0.248	0.049	-1.09	1.462	10
	18-24	0.05 ± 0.10	20.15	2.666	9.946	0.372	-0.291	-0.013	-1.34	1.455	13
	24-30	0.04 ± 0.70	27.46	2.651	9.663	0.395	-0.303	0.098	-1.71	1.472	9
(135)-(225)	0-6	0.07 ± 0.90	5.31	2.711	9.372	0.391	0.185	-0.445	-0.82	1.440	4
	6-12	0.07 ± 0.70	9.00	2.729	9.427	0.392	0.180	-0.444	-0.89	1.428	8
	12-18	0.08 ± 0.50	15.46	2.780	9.287	0.370	0.200	-0.440	-0.85	1.409	10
	18-24	0.06 ± 0.70	19.45	2.711	9.851	0.354	0.148	-0.410	-1.20	1.403	4
	24-30	0.09 ± 0.10	27.15	2.849	9.468	0.321	0.173	-0.404	-1.47	1.389	1

TABLE IV. The bins and the center-of-mass virtual-photoproduction cross sections for the reaction $\gamma_v + p \rightarrow \pi^+ + n$ off a deuterium target. The uncertainties are statistical only. N is the number of events in the bin. The cross sections shown have been radiatively corrected by multiplying the measured cross sections with the factor RAD.

ϕ (deg)	θ (deg)	$\frac{d\sigma}{d\Omega_r} \left(\frac{\mu\text{b}}{\text{sr}} \right)$	θ (deg)	W (GeV)	Q^2 (GeV ²)	ϵ	$\epsilon \cos 2\phi$	$\left[\frac{\epsilon(\epsilon+1)}{2} \right]^{1/2} \cos \phi$	t (GeV ²)	RAD	N
(a) Data point 1 (D_2)											
All	0-3	2.38 ± 0.28	1.94	2.099	1.201	0.468	-0.032	0.111	-0.08	1.324	87
(-135)-(-45)	0-3	2.31 ± 0.51	1.78	2.104	1.187	0.465	-0.308	0.076	-0.08	1.321	23
	3-6	2.74 ± 0.34	4.68	2.096	1.210	0.468	-0.326	-0.007	-0.08	1.320	79
	6-9	2.62 ± 0.31	7.44	2.119	1.183	0.453	-0.288	-0.057	-0.09	1.318	86
	9-12	2.19 ± 0.29	10.21	2.113	1.203	0.458	-0.281	0.029	-0.11	1.320	75
	12-15	1.91 ± 0.30	13.26	2.124	1.177	0.450	-0.299	-0.003	-0.13	1.317	50
	15-18	2.31 ± 0.40	16.44	2.104	1.202	0.462	-0.308	0.073	-0.17	1.319	36
	18-21	2.43 ± 0.65	19.25	2.071	1.225	0.485	-0.347	0.162	-0.20	1.324	16
	21-24	1.54 ± 1.14	21.50	2.021	1.375	0.499	-0.168	0.351	-0.24	1.336	2
(-45)-(45)	0-3	2.73 ± 0.57	2.03	2.073	1.229	0.482	0.277	0.527	-0.08	1.323	29
	3-6	2.63 ± 0.35	4.66	2.062	1.237	0.492	0.327	0.550	-0.09	1.329	65
	6-9	2.40 ± 0.32	7.35	2.031	1.274	0.511	0.323	0.558	-0.10	1.333	71
	9-12	2.41 ± 0.35	10.50	2.005	1.293	0.528	0.311	0.563	-0.13	1.338	68
	12-15	1.91 ± 0.38	13.46	1.980	1.307	0.544	0.315	0.572	-0.15	1.342	36
	15-18	1.83 ± 0.45	16.81	1.943	1.352	0.566	0.281	0.572	-0.19	1.347	18
	18-21	1.47 ± 0.69	19.45	1.943	1.347	0.569	0.242	0.559	-0.23	1.347	5
	21-24	0.92 ± 0.97	22.70	1.900	1.359	0.592	0.305	0.597	-0.26	1.347	1
(45)-(135)	0-3	2.18 ± 0.48	1.89	2.119	1.175	0.460	-0.332	-0.044	-0.08	1.321	23
	3-6	2.77 ± 0.36	4.56	2.116	1.204	0.454	-0.283	0.047	-0.08	1.321	93
	6-9	2.09 ± 0.25	7.52	2.098	1.207	0.464	-0.314	0.004	-0.09	1.319	92
	9-12	1.84 ± 0.23	10.35	2.109	1.191	0.463	-0.317	0.045	-0.11	1.321	73
	12-15	2.70 ± 0.33	13.46	2.100	1.204	0.468	-0.311	0.088	-0.13	1.321	77
	15-18	2.45 ± 0.44	16.59	2.066	1.235	0.491	-0.305	0.173	-0.16	1.325	39
	18-21	1.48 ± 0.58	18.85	2.070	1.215	0.489	-0.295	0.163	-0.19	1.324	7
	21-24	4.61 ± 3.28	22.43	1.936	1.350	0.572	-0.061	0.448	-0.22	1.339	2
(135)-(225)	0-3	2.25 ± 0.69	2.08	2.109	1.212	0.458	0.322	-0.530	-0.08	1.317	12
	3-6	2.61 ± 0.47	4.64	2.146	1.153	0.437	0.297	-0.511	-0.08	1.312	42
	6-9	1.51 ± 0.33	7.40	2.193	1.112	0.402	0.240	-0.472	-0.07	1.307	31
	9-12	2.06 ± 0.41	10.22	2.195	1.121	0.395	0.251	-0.472	-0.09	1.301	32
	12-15	0.83 ± 0.42	13.37	2.230	1.081	0.375	0.174	-0.431	-0.11	1.296	10
	15-18	0.59 ± 0.44	15.42	2.257	1.086	0.350	0.341	-0.483	-0.14	1.288	2
(b) Data point 2 (D_2)											
All	0-3	1.37 ± 0.18	2.08	2.659	1.947	0.345	0.003	0.060	-0.08	1.406	70
(-135)-(-45)	0-3	1.11 ± 0.29	2.17	2.670	1.923	0.337	-0.222	0.076	-0.07	1.402	16
	3-6	1.02 ± 0.18	4.65	2.668	1.968	0.332	-0.222	0.052	-0.09	1.402	44
	6-9	1.07 ± 0.16	7.43	2.644	2.021	0.342	-0.207	0.047	-0.11	1.400	53
	9-12	0.69 ± 0.13	10.24	2.632	2.022	0.350	-0.197	0.065	-0.14	1.400	29
	12-15	0.64 ± 0.17	13.43	2.625	2.050	0.355	-0.216	0.122	-0.19	1.404	19
	15-18	0.36 ± 0.24	16.18	2.538	2.112	0.417	-0.127	0.316	-0.24	1.419	5
(-45)-(45)	0-3	1.35 ± 0.32	1.97	2.636	2.021	0.351	0.249	0.448	-0.08	1.406	20
	3-6	0.95 ± 0.18	4.50	2.604	2.089	0.367	0.259	0.460	-0.10	1.413	40
	6-9	1.08 ± 0.17	7.39	2.577	2.116	0.380	0.232	0.456	-0.12	1.419	50
	9-12	0.83 ± 0.15	10.56	2.529	2.167	0.408	0.255	0.480	-0.16	1.426	34
	12-15	0.76 ± 0.21	13.60	2.489	2.269	0.425	0.212	0.474	-0.20	1.433	19
	15-18	0.74 ± 0.27	16.03	2.457	2.312	0.445	0.221	0.489	-0.25	1.438	8
18-21	0.66 ± 0.48	18.69	2.489	2.208	0.444	0.097	0.442	-0.29	1.431	2	

TABLE IV. (Continued)

ϕ (deg)	θ (deg)	$\frac{d\sigma}{d\Omega_{\pi}} \left(\frac{\mu\text{b}}{\text{sr}} \right)$	θ (deg)	W (GeV)	Q^2 (GeV ²)	ϵ	$\epsilon \cos 2\phi$	$\left[\frac{\epsilon(\epsilon+1)}{2} \right]^{1/2} \cos \phi$	t (GeV ²)	RAD	N
(b) Data point 2 (D ₂)											
(45)–(135)	0–3	1.24 ± 0.33	2.14	2.675	1.881	0.342	–0.210	0.003	–0.07	1.402	20
	3–6	1.29 ± 0.20	4.63	2.639	2.009	0.346	–0.220	0.029	–0.09	1.400	48
	6–9	0.80 ± 0.13	7.29	2.672	1.957	0.333	–0.218	–0.002	–0.10	1.399	45
	9–12	0.72 ± 0.14	10.31	2.621	2.031	0.358	–0.242	0.081	–0.13	1.401	35
	12–15	0.61 ± 0.16	13.60	2.632	1.994	0.359	–0.259	0.058	–0.18	1.400	20
	15–18	0.81 ± 0.30	16.58	2.571	2.171	0.382	–0.230	0.152	–0.23	1.406	8
(135)–(225)	0–3	2.32 ± 0.66	2.04	2.654	1.965	0.350	0.212	–0.432	–0.08	1.397	14
	3–6	1.25 ± 0.32	4.35	2.675	1.940	0.333	0.209	–0.423	–0.08	1.390	17
	6–9	1.81 ± 0.38	7.45	2.744	1.791	0.297	0.191	–0.396	–0.08	1.382	32
	9–12	0.77 ± 0.27	10.59	2.763	1.780	0.278	0.188	–0.385	–0.13	1.372	9
	12–15	0.40 ± 0.29	12.84	2.786	1.855	0.256	0.187	–0.373	–0.18	1.365	2

TABLE V. The bins and the center-of-mass virtual-photoproduction cross sections for the reaction $\gamma_v + n \rightarrow \pi^- + p$ off a deuterium target. The uncertainties are statistical only. N is the number of events in the bin. The cross sections shown have been radiatively corrected by multiplying the measured cross sections with the factor RAD.

ϕ (deg)	θ (deg)	$\frac{d\sigma}{d\Omega_{\pi}} \left(\frac{\mu\text{b}}{\text{sr}} \right)$	θ (deg)	W (GeV)	Q^2 (GeV ²)	ϵ	$\epsilon \cos 2\phi$	$\left[\frac{\epsilon(\epsilon+1)}{2} \right]^{1/2} \cos \phi$	t (GeV ²)	RAD	N
(a) Data point 1 (D ₂)											
All	0–3	2.41 ± 0.24	2.02	2.110	1.193	0.461	–0.015	0.127	–0.08	1.325	169
(–135)–(–45)	0–3	2.68 ± 0.50	2.06	2.112	1.189	0.462	–0.268	0.005	–0.07	1.321	59
	3–6	1.81 ± 0.23	4.64	2.108	1.194	0.462	–0.291	0.026	–0.09	1.321	101
	6–9	1.89 ± 0.22	7.58	2.129	1.174	0.448	–0.280	–0.020	–0.09	1.319	135
	9–12	1.65 ± 0.21	10.45	2.120	1.183	0.452	–0.293	0.030	–0.11	1.319	117
	12–15	1.41 ± 0.21	13.47	2.116	1.167	0.463	–0.295	0.055	–0.13	1.320	70
	15–18	0.95 ± 0.21	16.37	2.113	1.188	0.457	–0.304	0.088	–0.16	1.320	32
	18–21	1.18 ± 0.37	19.37	2.074	1.245	0.481	–0.257	0.173	–0.20	1.325	15
(–45)–(45)	0–3	3.21 ± 0.54	2.01	2.091	1.206	0.474	0.324	0.540	–0.08	1.324	55
	3–6	1.90 ± 0.26	4.55	2.067	1.228	0.488	0.306	0.540	–0.09	1.328	119
	6–9	2.32 ± 0.27	7.53	2.029	1.272	0.513	0.333	0.563	–0.12	1.333	129
	9–12	1.41 ± 0.21	10.55	2.004	1.304	0.527	0.330	0.569	–0.14	1.338	83
	12–15	1.48 ± 0.26	13.20	1.984	1.310	0.542	0.287	0.561	–0.16	1.342	62
	15–18	0.98 ± 0.28	16.23	1.957	1.355	0.552	0.348	0.589	–0.19	1.346	24
	18–21	0.86 ± 0.44	19.38	1.941	1.366	0.568	0.186	0.540	–0.23	1.353	7
(45)–(135)	0–3	1.77 ± 0.37	1.94	2.116	1.202	0.456	–0.245	0.009	–0.08	1.321	37
	3–6	2.11 ± 0.25	4.65	2.115	1.198	0.456	–0.296	–0.002	–0.08	1.321	131
	6–9	2.01 ± 0.21	7.48	2.111	1.195	0.461	–0.304	0.034	–0.09	1.321	162
	9–12	1.87 ± 0.20	10.26	2.114	1.177	0.462	–0.315	0.047	–0.11	1.321	135
	12–15	1.46 ± 0.20	13.33	2.100	1.206	0.467	–0.318	0.073	–0.13	1.320	95
	15–18	1.36 ± 0.27	16.09	2.085	1.213	0.479	–0.307	0.116	–0.15	1.322	46
	18–21	0.79 ± 0.36	18.98	2.064	1.254	0.488	–0.272	0.187	–0.19	1.325	11
	21–24	1.69 ± 1.78	22.13	1.976	1.311	0.542	–0.105	0.410	–0.23	1.337	2
(135)–(225)	0–3	1.66 ± 0.50	2.09	2.147	1.150	0.431	0.254	–0.492	–0.07	1.316	18
	3–6	2.13 ± 0.35	4.72	2.157	1.135	0.431	0.287	–0.505	–0.07	1.312	58
	6–9	1.45 ± 0.25	7.58	2.179	1.104	0.418	0.229	–0.476	–0.08	1.308	60
	9–12	1.31 ± 0.28	10.46	2.210	1.095	0.390	0.229	–0.461	–0.09	1.301	38
	12–15	1.67 ± 0.39	12.95	2.224	1.074	0.385	0.186	–0.442	–0.10	1.298	23
	15–18	0.45 ± 0.32	16.05	2.268	1.059	0.348	0.163	–0.411	–0.14	1.291	3

TABLE V. (Continued)

ϕ (deg)	θ (deg)	$\frac{d\sigma}{d\Omega_r}$ ($\frac{\mu\text{b}}{\text{sr}}$)	θ (deg)	W (GeV)	Q^2 (GeV 2)	ϵ	$\epsilon \cos 2\phi$	$\left[\frac{\epsilon(\epsilon+1)}{2}\right]^{1/2} \cos \phi$	t (GeV 2)	RAD	N
(b) Data point 2 (D_2)											
All	0-3	0.79 \pm 0.13	1.85	2.655	1.973	0.343	-0.070	0.119	-0.08	1.406	44
(-135)-(-45)	0-3	0.95 \pm 0.25	2.08	2.650	2.042	0.338	-0.249	0.075	-0.07	1.401	15
	3-6	0.86 \pm 0.15	4.18	2.654	1.962	0.344	-0.233	0.055	-0.08	1.402	36
	6-9	0.88 \pm 0.15	7.37	2.668	1.980	0.331	-0.206	0.032	-0.10	1.401	50
	9-12	0.50 \pm 0.11	10.48	2.644	2.003	0.349	-0.236	0.060	-0.14	1.401	24
	12-15	0.33 \pm 0.11	13.72	2.665	1.944	0.339	-0.256	0.058	-0.18	1.401	10
	15-18	0.10 \pm 0.10	15.25	2.709	1.821	0.323	-0.313	-0.057	-0.18	1.391	1
(-45)-(45)	0-3	0.69 \pm 0.22	1.32	2.651	1.953	0.348	0.221	0.436	-0.08	1.405	12
	3-6	0.77 \pm 0.14	4.49	2.576	2.130	0.379	0.231	0.455	-0.10	1.411	30
	6-9	0.59 \pm 0.12	7.08	2.557	2.136	0.395	0.251	0.472	-0.12	1.418	29
	9-12	0.58 \pm 0.12	10.45	2.513	2.215	0.413	0.273	0.490	-0.16	1.425	24
	12-15	0.75 \pm 0.18	13.09	2.499	2.294	0.418	0.206	0.466	-0.20	1.432	18
	15-18	0.59 \pm 0.23	16.22	2.478	2.271	0.430	0.194	0.470	-0.25	1.439	7
(45)-(135)	0-3	0.81 \pm 0.23	2.03	2.647	1.969	0.349	-0.237	0.050	-0.08	1.401	13
	3-6	0.75 \pm 0.14	4.52	2.654	1.964	0.345	-0.244	-0.022	-0.09	1.400	31
	6-9	0.62 \pm 0.11	7.38	2.683	1.886	0.333	-0.228	-0.001	-0.09	1.400	34
	9-12	0.51 \pm 0.11	10.49	2.654	1.949	0.346	-0.216	-0.024	-0.13	1.396	25
	12-15	0.39 \pm 0.12	13.53	2.613	2.013	0.367	-0.212	0.160	-0.18	1.407	13
	15-18	0.48 \pm 0.24	16.12	2.648	1.977	0.344	-0.264	-0.038	-0.21	1.389	6
(135)-(225)	0-3	0.59 \pm 0.30	2.02	2.714	1.787	0.324	0.271	-0.443	-0.06	1.397	4
	3-6	0.66 \pm 0.21	4.89	2.703	1.868	0.316	0.193	-0.407	-0.08	1.388	10
	6-9	0.86 \pm 0.23	7.08	2.732	1.840	0.306	0.215	-0.411	-0.09	1.383	15
	9-12	0.78 \pm 0.25	9.85	2.784	1.745	0.269	0.186	-0.378	-0.11	1.373	10
	12-15	0.36 \pm 0.26	13.24	2.765	1.739	0.294	0.048	-0.332	-0.15	1.373	2

TABLE VI. Separation of virtual-photon cross section for the reaction $\gamma_p p \rightarrow \pi^+ n$ into transverse component A and longitudinal component C .

$\langle Q^2 \rangle$ (GeV 2)	$\langle W \rangle$ (GeV)	$\langle \theta \rangle$ (deg)	A ($\mu\text{b}/\text{sr}$)	C ($\mu\text{b}/\text{sr}$)
1.19	2.15	1.96	1.06 \pm 0.50	3.82 \pm 0.76
		4.59	1.54 \pm 0.27	2.85 \pm 0.41
		7.56	1.83 \pm 0.23	1.92 \pm 0.34
		10.45	1.69 \pm 0.22	1.46 \pm 0.31
		13.39	1.42 \pm 0.25	1.15 \pm 0.33
2.00	2.65	1.93	0.98 \pm 0.28	0.76 \pm 0.46
		4.51	0.85 \pm 0.17	0.93 \pm 0.29
		7.49	0.39 \pm 0.14	1.19 \pm 0.19
		10.36	0.86 \pm 0.15	0.25 \pm 0.23
		13.42	0.41 \pm 0.16	0.41 \pm 0.23
3.32	2.65	16.19	0.53 \pm 0.34	0.04 \pm 0.45
		1.80	0.36 \pm 0.25	0.49 \pm 0.46
		4.69	0.25 \pm 0.18	0.79 \pm 0.38
		7.48	0.57 \pm 0.13	0.12 \pm 0.28
		10.63	0.64 \pm 0.11	-0.20 \pm 0.20
13.56	0.56 \pm 0.13	-0.16 \pm 0.23		
16.25	0.39 \pm 0.12	0.08 \pm 0.20		
19.45	0.47 \pm 0.13	-0.36 \pm 0.19		

Table VI lists these cross sections together with the averages of various kinematical parameters, and Fig. 3, a reproduction from Ref. 2, shows the dependence of A and C on θ together with the prediction of the dispersion-theory model¹⁰ which formed the basis of our earlier evaluations of the pion form factor.³⁻⁵ While the overall normalization of the predicted longitudinal cross section, C , depends directly on the chosen value for the pion form factor, the curves for the transverse cross section, A , are absolute predictions of the model. The dispersion-theory model predictions sizably underestimate the measured transverse cross section and this discrepancy becomes larger as Q^2 increases. In our earlier paper,² we found that the Q^2 dependence of the forward transverse cross section in the region $0 < Q^2 < 3.3$ GeV 2 was satisfactorily reproduced by the Q^2 dependence of the total virtual-photon production cross section. A fit to the data with $\theta < 3^\circ$ and $W = 2.65$ GeV gave the result $A = 0.025 \sigma_{\text{tot}} \text{ sr}^{-1}$. Figure 4 shows a plot of A and C/A versus Q^2 for $W = 2.65$ GeV and $\theta < 3^\circ$ together with the dispersion-theory predictions and the fit using the Q^2 dependence of the total virtual-

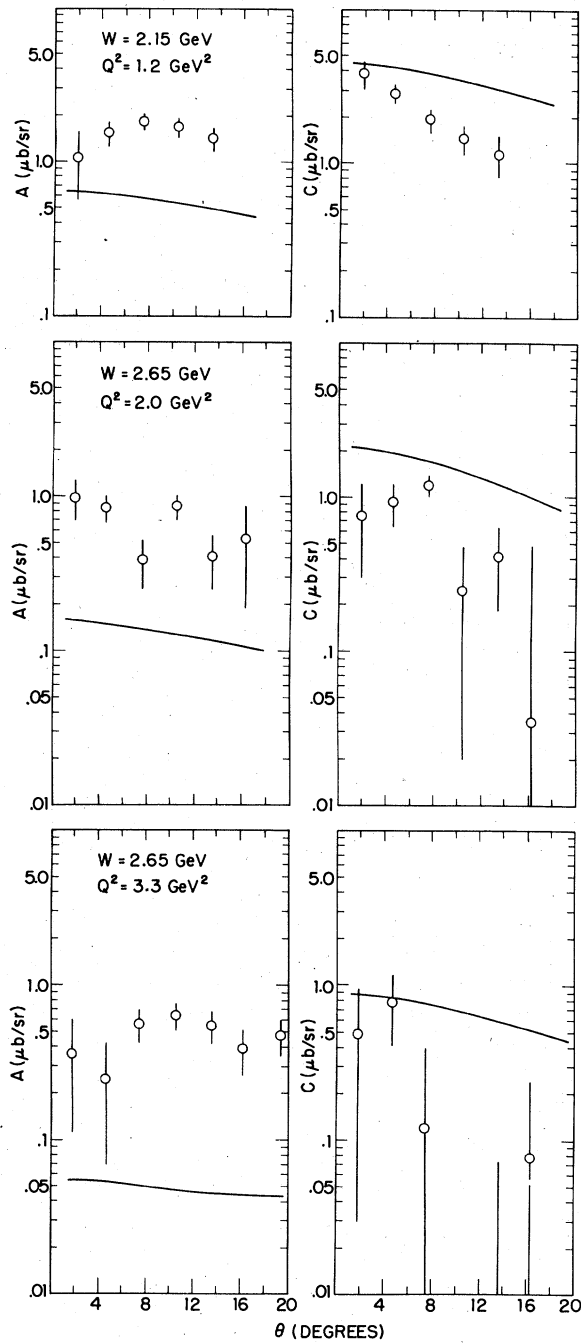


FIG. 3. The angular dependence of the transverse and longitudinal components A and C of the cross section for the reaction $\gamma_v p \rightarrow \pi^+ n$. The solid curves are the dispersion-theory predictions using $F_p = 1/(1+Q^2/0.471)$. This figure is reproduced from Ref. 2.

photoproduction cross section. Gutbrod and Kramer¹⁵ reached a similar conclusion by analyzing the measured Q^2 dependence of the longitudinal-transverse interference term, D .

The failure of the dispersion-theory model to re-

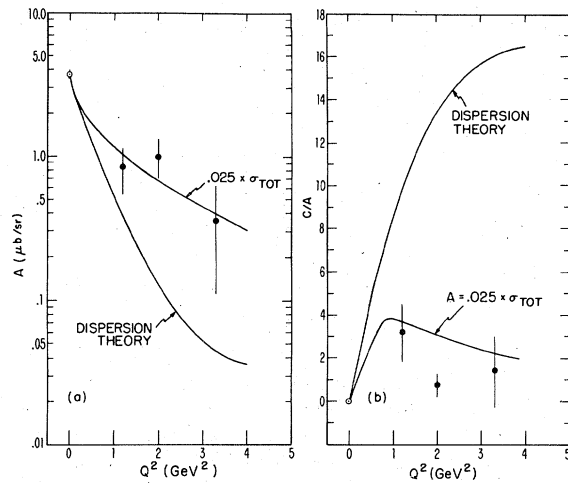


FIG. 4. (a) The Q^2 dependence of the transverse component A for $W = 2.65$ GeV and $\theta < 3^\circ$. The solid curves are the dispersion-theory prediction and a dependence on Q^2 which is the same as that found experimentally for the virtual-photon-proton total cross section. (b) The ratio C/A as a function of Q^2 . The solid curves were obtained using in one case the dispersion-theory prediction for C and A and, in the other, the dispersion-theory prediction for C together with the expression $(0.025 \text{ sr}^{-1})\sigma_{\text{tot}}$ for A (figure produced from Ref. 2).

produce the observed transverse cross section is at least partly due to the assumption that only isovector photons contribute to the single-pion electroproduction process. Previous measurements⁵ established the presence of a sizable isoscalar component which, for fixed W , increases with Q^2 . This isoscalar component is likely to be contained entirely in the transverse amplitudes since the main contributor to the longitudinal amplitude, the pion-exchange pole term, is purely isovector.

In order to determine the pion form factor from the data, we have followed a procedure which avoids some of the problems associated with the theoretical models. The main ingredients are as follows:

(1) The use of data with $\theta < 3^\circ$ so that the $\cos\phi$ and $\cos 2\phi$ terms are small. This minimizes the contributions of the interference terms so that terms B and D in Eq. (3) can be neglected.

(2) The assumption that the amplitude due to longitudinal photons is given by the t -channel one-pion-exchange Born term.

(3) The assumption that for $\theta \approx 0^\circ$, the Q^2 dependence of the part of the cross section due to transverse photons, A , is the same as that for the total virtual-photoproduction cross section. It is also assumed that the W dependence of A is the same as the W dependence of the s - and u -channel Born terms.

TABLE VII. The values of the pion form factor derived from the data of this and earlier experiments (Refs. 3-5) using the measured Q^2 dependence of the transverse cross section, term A in the table, and the t -channel Born term.

$\langle Q^2 \rangle$ (GeV ²)	$\langle W \rangle$ (GeV)	$\langle \epsilon \rangle$	$\frac{d\sigma}{d\Omega}$ ($\frac{\mu\text{b}}{\text{sr}}$)	A ($\frac{\mu\text{b}}{\text{sr}}$)	F_π
(a) CEA data (Ref. 3)					
0.18	2.15	0.85	7.15 ± 0.34	3.945	0.850 ± 0.044
0.29	2.15	0.83	8.05 ± 0.44	3.320	0.634 ± 0.029
0.40	2.15	0.87	8.90 ± 0.34	2.921	0.570 ± 0.016
0.79	2.15	0.83	6.99 ± 0.37	2.080	0.384 ± 0.014
1.19	2.15	0.79	3.54 ± 0.28	1.570	0.238 ± 0.017
(b) Earlier Cornell data (Ref. 4)					
0.62	2.67	0.87	5.15 ± 0.25	1.488	0.445 ± 0.016
1.07	2.89	0.81	3.53 ± 0.31	0.902	0.309 ± 0.019
1.20	2.65	0.86	3.81 ± 0.23	0.993	0.269 ± 0.012
1.31	2.46	0.90	3.50 ± 0.29	1.098	0.242 ± 0.015
1.20	2.14	0.94	4.43 ± 0.29	1.579	0.262 ± 0.014
2.01	2.66	0.82	1.59 ± 0.17	0.655	0.154 ± 0.014
(c) Later Cornell data (Ref. 5)					
1.22	2.14	0.95	5.08 ± 0.74	1.558	0.290 ± 0.030
1.20	3.08	0.82	3.09 ± 0.31	0.732	0.294 ± 0.019
1.71	3.09	0.79	2.52 ± 0.32	0.551	0.238 ± 0.020
3.30	2.66	0.82	0.77 ± 0.17	0.390	0.102 ± 0.023
1.99	2.14	0.94	2.28 ± 0.29	1.071	0.179 ± 0.021
3.99	2.14	0.88	0.51 ± 0.16	0.513	0.004 ± 0.678
(d) This experiment					
1.18	2.11	0.47	2.97 ± 0.27	1.646	0.256 ± 0.026
1.94	2.67	0.33	1.26 ± 0.15	0.673	0.193 ± 0.025
3.33	2.63	0.39	0.52 ± 0.10	0.397	0.086 ± 0.033
6.30	2.66	0.40	0.19 ± 0.05	0.149	0.059 ± 0.030
9.77	2.63	0.40	0.12 ± 0.03	0.064	0.070 ± 0.019

This method was used to determine the pion form factor from the new data and the data reported earlier.³⁻⁵

The results are presented in Table VII and, graphically, in Fig. 5. It should be noted that for values of Q^2 greater than 4 GeV² the transverse cross section is determined from an extrapolation of the low- Q^2 data and so these points are probably the least reliable. The uncertainties shown in the table and figure are statistical only.

We have fitted the data listed in Table VII to the simple pole form

$$F(Q^2) = (1 + Q^2/m_V^2)^{-1}. \quad (4)$$

The result is

$$m_V^2 = 0.462 \pm 0.012 \text{ GeV}^2$$

with a χ^2 of 37.7 for 21 degrees of freedom. This

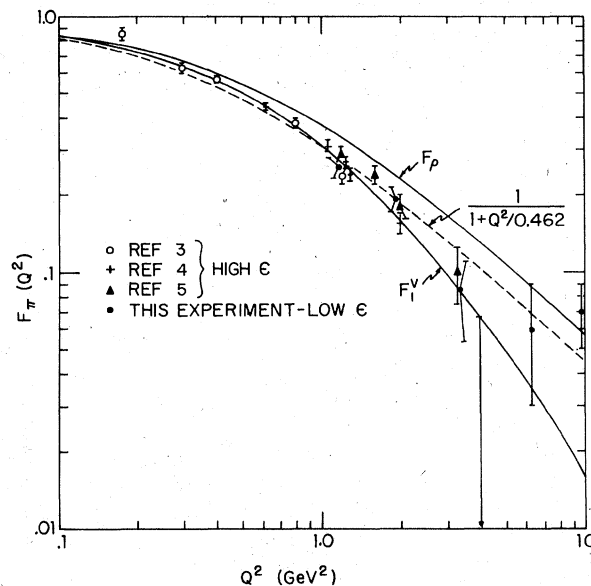


FIG. 5. The values of the pion form factor derived from the data reported in this and earlier experiments using the measured transverse cross section and the t -channel Born term. Also shown are the ρ pole form factor and the isovector nucleon form factor (solid lines), as well as the result of a simple pole fit (broken line).

fit gives for the electromagnetic radius of the pion

$$\langle r_\pi^2 \rangle^{1/2} = 0.711 \pm 0.009 \text{ F}.$$

To determine the uncertainty in the mass parameter, m_V^2 , and the pion radius due to the estimated 6% overall normalization uncertainty, we made least-squares fits to the expressions

$$0.97/(1 + Q^2/m_V^2)$$

and

$$1.03/(1 + Q^2/m_V^2).$$

These two fits gave respectively for the mass parameter

$$m_V^2 = 0.484 \pm 0.014 \text{ GeV}^2$$

and

$$m_V^2 = 0.442 \pm 0.010 \text{ GeV}^2.$$

From the overall variation we then assigned the following errors to the mass parameter:

$$m_V^2 = 0.462 \pm 0.012 \pm 0.021 \text{ GeV}^2,$$

and to the pion form factor:

$$\langle r_\pi^2 \rangle^{1/2} = 0.711 \pm 0.009 \pm 0.016 \text{ F}.$$

Here the first error denotes the statistical uncertainty and the second the systematic uncertainty. Adding the two uncertainties in quadrature gives

TABLE VIII. A summary of the more recent determinations of the pion electromagnetic radius by the several methods that have been used for this purpose.

Group	Method	$\langle r_\pi^2 \rangle^{1/2}$ (F)
Berezhnev <i>et al.</i> (1973) Ref. 16	Inverse electroproduction $n + p \rightarrow e^+ e^- n$	0.73 \pm 0.13
Adylov <i>et al.</i> (1974) Ref. 17	Pion-electron scattering $E = 50$ GeV	0.78 \pm 0.10
Dubnicka and Dunbrajs (1974) Ref. 18	Alternate analysis of data from Adylov <i>et al.</i> (1974)	0.71 \pm 0.05
Bebek <i>et al.</i> (1976) Ref. 5	Electroproduction above resonance region up to $Q^2 = 4$ GeV ²	0.704 \pm 0.025
Bardin <i>et al.</i> (1977) Ref. 19	Electroproduction in resonance region up to $Q^2 = 0.12$ GeV ²	0.74 ^{+0.11} _{-0.13}
Quenzer <i>et al.</i> (1977) Ref. 20	Colliding-beam measurement of $e^+ e^- \rightarrow \pi^+ \pi^-$	0.676 \pm 0.008
Dally <i>et al.</i> (1977) Ref. 21	Pion-electron scattering $E = 100$ GeV	0.56 \pm 0.04
This experiment	Electroproduction above resonance region up to $Q^2 = 10$ GeV ²	0.711 \pm 0.018

$$m_\nu^2 = 0.462 \pm 0.024 \text{ GeV}^2,$$

$$\langle r_\pi^2 \rangle^{1/2} = 0.711 \pm 0.018 \text{ F}.$$

Table VIII summarizes the recently reported values of the pion radius and the techniques through which they were obtained.¹⁶⁻²¹ The agreement between the more precise measurements is poor and suggests additional uncertainties in the models used to determine the pion radius from the data. It is especially disturbing that the most recent pion-electron scattering experiment, which was carried out by a UCLA-Notre Dame-Pittsburgh-Fermilab-Dubna group at Fermilab, gives a value so much lower than the recent Orsay colliding-beam experiment and this electroproduction experiment.

A DESY-Hamburg group²² has recently reported an experiment in which they carried out a longitudinal-transverse separation at the (W, Q^2) point (2.19 GeV, 0.70 GeV²). They found a value for A which is larger than expected from the simple dispersion-theory model and which has a weak dependence on momentum transfer in agreement with the results of this experiment. They used the Gutbrod-Kramer generalized Born term model¹⁵ to fit their data and found $F_\pi = 0.42 \pm 0.015$. This is to be compared with the value 0.40 calculated from Eq. (4).

IV. CONCLUSION

We have devised a simple scheme for the evaluation of the pion form factor in the spacelike region

TABLE IX. A comparison of the values for the pion factor determined in this analysis and the earlier analyses (Ref. 5) using Berends theory and correcting empirically for the isoscalar component.

Data point		F_π	
$\langle Q^2 \rangle$ (GeV ²)	$\langle W \rangle$ (GeV)	Earlier analysis	This analysis
(a) CEA data (Ref. 3)			
0.18	2.15	0.786 \pm 0.045	0.850 \pm 0.044
0.29	2.15	0.606 \pm 0.028	0.634 \pm 0.029
0.40	2.15	0.550 \pm 0.015	0.570 \pm 0.016
0.79	2.15	0.380 \pm 0.013	0.384 \pm 0.014
1.19	2.15	0.256 \pm 0.013	0.238 \pm 0.017
(b) Earlier Cornell data (Ref. 4)			
0.62	2.67	0.453 \pm 0.014	0.445 \pm 0.016
1.07	2.89	0.321 \pm 0.017	0.309 \pm 0.019
1.20	2.65	0.279 \pm 0.010	0.269 \pm 0.012
1.31	2.46	0.252 \pm 0.012	0.242 \pm 0.015
1.20	2.14	0.269 \pm 0.011	0.262 \pm 0.014
2.01	2.66	0.174 \pm 0.010	0.154 \pm 0.014
(c) Later Cornell data (Ref. 5)			
1.22	2.14	0.292 \pm 0.026	0.290 \pm 0.030
1.20	3.08	0.305 \pm 0.017	0.294 \pm 0.019
1.71	3.09	0.246 \pm 0.017	0.238 \pm 0.020
3.30	2.66	0.123 \pm 0.015	0.102 \pm 0.023
1.99	2.14	0.199 \pm 0.015	0.179 \pm 0.021
3.99	2.14	0.101 \pm 0.019	0.004 \pm 0.678

for Q^2 up to 10 GeV². This procedure uses the t -channel Born term for the cross section due to longitudinal photons and the measured Q^2 dependence of the transverse cross section. The newly calculated values of the pion form factor are slightly lower than ones previously reported. Table IX gives a comparison of the earlier reported values for the pion form factor⁵ and the results of the new analysis reported here. Although the values are compatible with a simple pole expression, a form such as $F_\pi = F_1^\nu$ cannot be ruled out. The main limitation in this analysis is the poor knowledge of the transverse term A over the full range in Q^2 and the necessity of relying on relatively low-precision measurements at three (W , Q^2) points.

The absence of a theory which gives an accurate description of exclusive pion electroproduction precludes a precise determination of the pion form factor in the region of large spacelike Q^2 . Our method of extracting the form factor relies heavily

on the assumption that t -channel pion exchange is entirely responsible for the longitudinal cross section and that it can be adequately described by the Born term approximation. Previously published measurements² of the longitudinal cross section indicate that the angular distribution, even for small momentum transfers t , disagrees with the one expected on the basis of t -channel pion exchange. Since the minimum momentum transfer, t_{\min} , for our data increases with Q^2 , our form-factor values for large Q^2 are subject to some uncertainty.

ACKNOWLEDGMENTS

We would like to acknowledge the support of Professor Boyce McDaniel, the staff of the Wilson Synchrotron Laboratory, and the staff of the Harvard High Energy Physics Laboratory. This work was supported by the National Science Foundation (Cornell) and the Department of Energy (Harvard).

*Present address: Fermi National Acceleratory Laboratory, P. O. Box 500, Batavia, Illinois 60510.

†Present address: Physics Department, Columbia University, New York, N. Y. 10027.

‡Present address: 36 Webb Street, Lexington, Mass. 02173.

§Present address: Clinton P. Anderson Laboratory, Los Alamos, New Mexico 87545.

¹For a general review of our present theoretical understanding of the pion form factor see M. Gourdin, Phys. Rep. **11C**, 29 (1974).

²C. J. Bebek, A. Browman, C. N. Brown, K. M. Hanson, S. D. Holmes, R. V. Kline, D. Larson, F. M. Pipkin, S. W. Raither, A. Silverman, and L. K. Sisterson, Phys. Rev. Lett. **37**, 1326 (1976).

³C. N. Brown, C. R. Canizares, W. E. Cooper, A. M. Eisner, G. J. Feldman, C. A. Lichtenstein, L. Litt, W. Lockeretz, V. B. Montana, and F. M. Pipkin, Phys. Rev. D **8**, 92 (1973).

⁴C. J. Bebek, C. N. Brown, M. Herzlinger, S. Holmes, C. A. Lichtenstein, F. M. Pipkin, L. K. Sisterson, D. Andrews, K. Berkelman, D. G. Cassel, and D. L. Hartill, Phys. Rev. D **9**, 1229 (1974).

⁵C. J. Bebek, C. N. Brown, M. Herzlinger, S. D. Holmes, C. A. Lichtenstein, F. M. Pipkin, S. Raither, and L. K. Sisterson, Phys. Rev. D **13**, 25 (1976).

⁶A. Bartl and P. Urban, Acta. Phys. Austriaca **24**, 139 (1966).

⁷C. J. Bebek, C. N. Brown, R. V. Kline, F. M. Pipkin, S. W. Raither, L. K. Sisterson, A. Browman, K. M. Hanson, D. Larson, and A. Silverman, Phys. Rev. D **16**, 1986 (1977).

⁸L. N. Hand, Phys. Rev. **129**, 1834 (1963).

⁹L. Hulthén and M. Sugawara, *Handbuch der Physik*, edited by S. Flügge (Springer, Berlin, 1957), Vol. XXXIX, p. 1.

¹⁰F. A. Berends, Phys. Rev. D **1**, 2590 (1970).

¹¹R. C. E. Devenish and D. H. Lyth, Phys. Rev. D **5**, 47

(1972).

¹²W. Schmidt, Report No. DESY 71/72, 1971 (unpublished).

¹³B. H. Kellett, Nucl. Phys. **B38**, 573 (1972).

¹⁴H. Fraas and D. Schildknecht, Phys. Lett. **35B**, 72 (1971).

¹⁵F. Gutbrod and G. Kramer, Nucl. Phys. **B49**, 461 (1972).

¹⁶S. F. Bereznev, L. S. Vertogradov, A. V. Dem'yanov, A. V. Kulikov, A. V. Kuptsov, G. G. Mkrtchyan, L. L. Nemenov, G. I. Smirnov, D. M. Khazins, and Yu. M. Chirkin, Yad. Fiz. **16**, 185 (1972) [Sov. J. Nucl. Phys. **16**, 99 (1973)].

¹⁷G. T. Adylov, I. K. Aliev, D. Yu. Bardin, W. Gajewski, I. Ion, B. A. Kulakov, G. V. Micelmacher, B. Niczyporuk, T. S. Nigmanov, E. N. Tsyganov, M. Turala, A. S. Vodopianov, K. Wala, E. Dally, D. Drickey, A. Liberman, P. Shepard, J. Tompkins, C. Buchanan, and J. Poirier, Phys. Lett. **51B**, 402 (1974).

¹⁸S. Dubnicka and O. V. Dumbrajs, Phys. Lett. **53B**, 285 (1974).

¹⁹G. Bardin, J. Duclos, A. Magnon, B. Michel, and J. C. Montret, Nucl. Phys. **B120**, 45 (1977).

²⁰A. Quenzer, M. Ribes, F. Rumpf, J. L. Bertrand, J. C. Bizot, R. L. Chase, A. Cordier, B. Delcourt, P. Eschstruth, F. Fulda, G. Grosdidier, J. Haissinski, J. Jeanjean, M. Jeanjean, R. J. Madaras, J. L. Mosnou, and J. Perez-Y-Jorba, contributed paper to the 1977 International Symposium on Lepton and Photon Interactions at High Energies, Hamburg, 1977 (unpublished).

²¹E. B. Dally, D. J. Drickey, J. M. Hauptman, C. F. May, D. H. Stork, J. A. Poirier, C. A. Rey, R. J. Wojslaw, P. F. Shepard, A. J. Lennox, J. C. Tompkins, T. E. Toohig, A. A. Wehmann, I. X. Ioan, T. S. Nigmanov, E. N. Tsyganov, and A. S. Vodopianov, Phys. Rev. Lett. **39**, 1176 (1977).

²²P. Brauel, T. Canzler, D. Cords, R. Felst, G. Grindhammer, M. Helm, W.-D. Kollmann, M. Krehbiel, and M. Schädlich, Phys. Lett. **69B**, 253 (1977).